



# **A new pathway for the re-equilibration of micellar surfactant solutions**

**by**

**I. M. Griffiths  
C. J. W. Breward  
D. M. Colegate  
P. J. Dellar  
P. D. Howell  
C. D. Bain**



# A new pathway for the re-equilibration of micellar surfactant solutions

I. M. Griffiths,<sup>a†</sup> C. J. W. Breward,<sup>a</sup> D. M. Colegate,<sup>a</sup> P. J. Dellar,<sup>a</sup> P. D. Howell,<sup>a</sup> and C. D. Bain<sup>\*b</sup>

Received Xth XXXXXXXXXXXX 20XX, Accepted Xth XXXXXXXXXXXX 20XX

First published on the web Xth XXXXXXXXXXXX 200X

DOI: 10.1039/b000000x

Micellar surfactant solutions are generally assumed to undergo restructuring via stepwise monomer loss following a dilution. This process is captured by the Becker–Döring equations, an infinite-dimensional system of ordinary differential equations for the concentration of each aggregate in solution. We reveal certain classes of surfactants, such as the non-ionic family  $C_nE_m$ , for which the predicted re-equilibration times via stepwise monomer loss are far greater than those observed experimentally. We investigate two alternative pathways for re-equilibration, first allowing for micelles to break down into two aggregate fragments rather than stepwise monomer release, and secondly by allowing aggregates to merge together to form large *super-micelles* that exceed the size of a proper micelle. While the former shows no discernible difference in the predicted time to re-equilibration, the latter provides an alternative pathway to re-equilibration: the formation of unstable super-micelles that break down to proper micelles via a cascade of stepwise monomer release. The new theory is shown to describe the re-equilibration of *any* surfactant system, with the conventional Becker–Döring theory forming a subset of the model that describes the behaviour of a small range of surfactant systems with high critical micelle concentrations and low aggregation numbers. The pathway proposed provides an essential mechanistic route to equilibrium.

## 1 Introduction

When surfactant exceeds a particular bulk concentration in solution, termed the *critical micelle concentration* (CMC), it becomes energetically favourable for aggregates or *micelles* to form. The micelles can have various sizes and shapes but for many simple surfactants with a single hydrocarbon chain the aggregates are approximately spherical and contain of the order of 100 monomers.<sup>1</sup> The distribution of aggregate sizes is localized around this optimum value with a half-width of the order of the square root of the aggregation number. Aggregates that are much smaller than the mean aggregation number are significantly less energetically favourable and consequently appear in much lower concentrations.<sup>2–5</sup>

Following dilution of the solution, for example by adding pure water, micelles must break down to replenish the monomer to the CMC. The breakdown process is conventionally assumed to occur via stepwise monomer gain or loss. This leads to the Becker–Döring description, an infinite-dimensional system of coupled nonlinear ordinary differential equations (ODEs) that describe the evolution of the concentration of each aggregate size.<sup>6,7</sup>

The re-equilibration process is characterized by two distinct

stages, commonly referred to as the  $\tau_1$  and  $\tau_2$  processes. In the  $\tau_1$  process, following dilution, the depleted monomer is replenished by the shedding of individual monomers from aggregates near micellar size, leading to a decrease in the dominant aggregate size. This occurs on a timescale of the order of microseconds.<sup>8</sup> The  $\tau_2$  process is characterized by the entire breakdown of some aggregates via stepwise monomer loss. Here, some of the monomers released remain in this form to replenish the monomer to the equilibrium, while the remainder associate with some of the aggregates that have not dissociated. This has the simultaneous impact of increasing the dominant aggregate size while decreasing the total concentration of surfactant contained in aggregates.

The relative timescales of the  $\tau_1$  and  $\tau_2$  processes are related to the proportion of the energetically unfavourable aggregates. For typical surfactants, the concentration of these aggregates is often many orders of magnitude lower than the concentration of proper micelles. This leads to extreme separation of timescales as a result of their high free energy, which severely restricts the flow of material through this region as micelles break down.<sup>6,7</sup> For some surfactants, experimentally observed re-equilibration timescales are very much shorter than this model would suggest: while the Becker–Döring theory predicts re-equilibration over timescales of the order of hundreds of years for certain polyoxyethylene glycol alkyl ether surfactants (such as  $C_{12}E_8$ ), stopped-flow experiments exhibit re-equilibration on the order of seconds.<sup>6,7,9</sup> The mechanism by

<sup>a</sup> Mathematical Institute, University of Oxford, 24–29 St Giles', Oxford, U.K.

<sup>†</sup> E-mail: [ian.griffiths@maths.ox.ac.uk](mailto:ian.griffiths@maths.ox.ac.uk)

<sup>b</sup> Department of Chemistry, Durham University, South Road, Durham, DH1 3LE, U.K.; E-mail: [c.d.bain@durham.ac.uk](mailto:c.d.bain@durham.ac.uk)

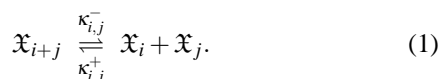
which a system re-equilibrates when subject to a non-small dilution, but one that leaves the bulk concentration above the CMC (so the system remains micellar), is thus unclear.

In this paper we explore the underlying breakdown kinetics of a surfactant system and propose a new pathway for complete micelle breakdown which does not involve aggregates in the low-concentration, high free-energy region. We begin in §2 by outlining the full discrete model for micellar aggregation and breakdown kinetics and the distributions observed in typical surfactant systems. In §3 we propose a continuum description which simplifies the model, providing a tractable model for analysis. Potential alternative pathways to re-equilibration that do not rely solely upon the conventional stepwise monomer loss route to re-equilibration are proposed and investigated in §4. We conclude by comparing the predictions of the model with the conventional theory that assumes only stepwise monomer loss, to determine the regimes under which the original theory accurately characterizes the route to equilibrium, and those for which re-equilibrium can only occur on a sensible timescale by including our new pathway.

## 2 A discrete model

### 2.1 The Smoluchowski equations

The Becker–Döring theory for aggregation and breakdown kinetics of micellar solutions makes the principal assumption that the process occurs via only stepwise monomer loss and gain. This assumption may be relaxed to allow for the coagulation of any two aggregates and likewise the fragmentation of an aggregate into any two components through the reversible reaction



Here  $\mathfrak{X}_n$  denotes the (molar) concentration of an aggregate containing  $n$  monomers, and  $\kappa_{i,j}^\pm$  are the association and dissociation rate coefficients with  $\kappa_{i,j}^\pm = \kappa_{j,i}^\pm$  by symmetry. The time evolution of such a system may be described by Smoluchowski theory,<sup>10</sup>

$$\frac{d\mathfrak{X}_n}{dt} = \sum_{i=1}^{n-1} \frac{1}{2} \left( \kappa_{i,n-i}^+ \mathfrak{X}_i \mathfrak{X}_{n-i} - \kappa_{i,n-i}^- \mathfrak{X}_n \right) - \sum_{i=1}^{\infty} \left( \kappa_{i,n}^+ \mathfrak{X}_i \mathfrak{X}_n - \kappa_{i,n}^- \mathfrak{X}_{i+n} \right), \quad (2)$$

for  $n \geq 2$ , where  $\mathfrak{X}_n(t)$  denotes the concentration at time  $t$ . The first summation corresponds to reaction (1) with  $j = n - i$ , which constitutes the formation of aggregates of size  $n$  from smaller aggregates (and the corresponding reverse reaction); the factor  $1/2$  appears to avoid double counting of equivalent

reactions with  $i$  and  $j$  interchanged. The second summation corresponds to reaction (1) with  $j = n$ , which represents the formation of aggregates of size  $n$  by the breakdown of a larger aggregate into two smaller components (and the corresponding reverse reaction).

The net bulk concentration of monomer contained in all aggregates is given by

$$\mathcal{C}_b = \sum_{n=1}^{\infty} n \mathfrak{X}_n. \quad (3)$$

Under the assumption that  $\mathcal{C}_b$  is conserved for all time, the free monomer concentration is determined by

$$\mathfrak{X}_1(t) = \mathcal{C}_b - \sum_{n=2}^{\infty} n \mathfrak{X}_n(t) = \mathfrak{X}_1(0) - \sum_{n=2}^{\infty} n (\mathfrak{X}_n(t) - \mathfrak{X}_n(0)). \quad (4)$$

Along with (2), this provides an infinite-dimensional system of ODEs for  $\mathfrak{X}_2(t), \mathfrak{X}_3(t), \dots$ . The solution of this system requires us to specify all the initial concentrations  $\mathfrak{X}_1(0), \mathfrak{X}_2(0), \dots$ .

Setting  $\kappa_{i,j}^\pm = 0$  when both  $i, j \neq 1$  corresponds to a system in which the coalescence between two aggregates (species composed of two or more monomers) cannot occur and (2) reduces to the Becker–Döring equations,<sup>11</sup>

$$\frac{d\mathfrak{X}_n}{dt} = \kappa_{1,n-1}^+ \mathfrak{X}_1 \mathfrak{X}_{n-1} - \kappa_{1,n-1}^- \mathfrak{X}_n - \kappa_{1,n}^+ \mathfrak{X}_1 \mathfrak{X}_n + \kappa_{1,n}^- \mathfrak{X}_{n+1}, \quad (5)$$

studied in this context in Griffiths *et al.*<sup>6,7</sup>

In this paper we propose modified mechanisms for the re-equilibration of a micellar solution following dilution, which lead to new forms for the association and dissociation rates,  $\kappa_{i,j}^\pm$ . The method by which these rate coefficients are determined is discussed below.

### 2.2 Determining the reaction rates

Diffusion-controlled reactions between two species  $\mathfrak{X}_i$  and  $\mathfrak{X}_j$  occur with a rate constant<sup>10,12</sup>

$$R_{i,j}^+ = 4\pi N_A \sigma_{i,j} (D_i + D_j), \quad (6)$$

where  $N_A$  is the Avogadro number,  $D_n$  represents the diffusion coefficient of an aggregate of size  $n$ , and  $\sigma_{i,j}$  is the collision radius. We may take  $\sigma_{i,j}$  to be the sum of the aggregate radii,  $r_i + r_j$  (with  $r_n$  proportional to  $n^{1/3}$ ), and the Stokes–Einstein equation provides a relation between the diffusion coefficient of an aggregate and its size, namely

$$D_n = \frac{k_B T}{6\pi\mu r_n}, \quad (7)$$

where  $k_B$  is the Boltzmann constant, and  $T$  and  $\mu$  are the temperature and viscosity of the solution. This provides

$$R_{i,j}^+ = \left( \frac{2k_B N_A T}{3\mu} \right) \frac{(i^{1/3} + j^{1/3})^2}{i^{1/3} j^{1/3}}. \quad (8)$$

The estimate (8) predicts rather weak dependence of the association rates upon aggregate size and we assume henceforth in this paper that the diffusion-controlled association rates  $R_{i,j}^+$  are all equal.

Ultrasonic adsorption studies suggest that monomer association proceeds at a rate close to the diffusion-controlled limit so that we can set  $\kappa_{i,j}^+ = R_{i,j}^+$ .<sup>13,14</sup> Such reaction rates are in line with spectroscopic stopped-flow experiments on the polyoxyethylene glycol alkyl ether surfactant  $C_nE_m$  series, where rapid re-equilibration is observed to occur before data acquisition begins, that is, on a timescale less than 10 ms.<sup>9</sup> However, while monomer association generally proceeds at a diffusion-controlled rate, it is anticipated that the association of two aggregates of size  $i, j \geq 2$  will have an additional activation barrier to overcome. Thus while it is safe to suppose that  $\kappa_{1,n}^+ = \kappa_{1,1}^+ = R_{1,1}^+$  for all  $n$  (there is no physical reason why the additional reactions should affect the rate of monomer uptake for any aggregate size), the form that  $\kappa_{i,j}^+$  for  $i, j \neq 1$  should take is less clear, and this forms the focus of our study in this paper.

The dissociation rates,  $\kappa_{i,j}^-$ , are not well characterized but may be determined by the following method, provided we know the association rates,  $\kappa_{i,j}^+$ , and the equilibrium distribution before dilution,  $\mathfrak{X}_n = \mathfrak{X}_n^*$  say. At equilibrium, the principle of microscopic reversibility requires that each mechanistic step in a reversible reaction must itself be in equilibrium, that is, each of the terms in the summations in (2) must be equivalently zero, and so we have that

$$\kappa_{i,j}^+ \mathfrak{X}_i^* \mathfrak{X}_j^* = \kappa_{i,j}^- \mathfrak{X}_{i+j}^*. \quad (9)$$

Equation (9) may be rearranged to provide an expression for the dissociation rates in terms of the association rates and equilibrium distribution,

$$\kappa_{i,j}^- = \left( \frac{\mathfrak{X}_i^* \mathfrak{X}_j^*}{\mathfrak{X}_{i+j}^*} \right) \kappa_{i,j}^+, \quad (10)$$

for  $i, j \geq 1$ .<sup>†</sup>

### 2.3 The equilibrium distribution

Determination of the equilibrium size distribution,  $\mathfrak{X}_n^*$ , for different surfactants and different micelle shapes is a subject of extensive debate. Since concentrations in the intermediate

aggregate region are orders of magnitude smaller than those close to the optimum aggregation number, there are no direct experimental methods available for their measurement. It is, however, possible to calculate an equilibrium aggregate size distribution from knowledge of the chemical potential differences between monomers in different sized aggregates. This may be done via Molecular Dynamics (MD) simulations<sup>15–17</sup> or by Molecular Thermodynamics (MT).<sup>5,18,19</sup> Either method predicts a distribution characterized by the following key features. Almost all surfactant material is contained within a region of *oligomers* (monomer, dimers, trimers, etc.) and a region of *proper micelles* close to the peak aggregation number. These are connected by an *intermediate region* containing a very low concentration of aggregates; see the solid line in Fig. 1.

The model we will present in §3 is valid for any equilibrium distribution  $\mathfrak{X}_n^*$  resembling that shown in Fig. 1, with surfactant concentrated in narrow neighbourhoods of  $n = 1$  and  $n = m$  (the peak aggregation number), separated by an intermediate region of very low concentration. However, to fix ideas here we focus on a particular fit to the equilibrium distribution, namely

$$\frac{\mathfrak{X}_n^*}{\mathfrak{X}_1^*} = A \exp(b - bn) + \frac{B}{m^{3/2}} \exp\left(-\beta m(n/m - 1)^2\right) + \frac{C}{m^2} \exp(-dn/m), \quad (11)$$

where  $A, B, C, b, \beta, d$  and  $m$  are fitting parameters. The first term represents the spike at  $n = 1$  and the small number of oligomers. The second term captures the distribution of proper micelles with a spread determined by  $\beta$ . The third term is a slowly decaying exponential which represents the concentration of intermediate aggregates: the value of  $C$  and  $d$  can be used to control the ratio of maximum to minimum aggregate concentrations. The scaling of the second and third terms by  $m^{-3/2}$  and  $m^{-2}$ , respectively, ensures that the importance of these terms, relative to each other and to the monomer concentration, depends on the coefficients  $A, B$  and  $C$  and not on the most probable aggregation number,  $m$ . The distribution (11) captures the key features predicted by MT illustrated in Fig. 1. In particular, the largeness of  $m$  ensures the high relative concentration of monomer to aggregates, as well as a narrow Gaussian spread around  $n = m$ .

We can fix two parameters, for example  $A$  and  $B$ , by requiring the right-hand side of (11) to be equal to 1 when  $n = 1$  and

<sup>†</sup> The magnitudes of the dissociation rates predicted by (10) are discussed in Appendix A.

by specifying the net concentration:

$$1 = A + \frac{B}{m^{3/2}} e^{-\beta(m-1)^2/m} + \frac{C}{m^2} e^{-d/m}, \quad (12)$$

$$C_b = \frac{\mathcal{C}_b}{\mathfrak{X}_1^*} = \frac{A}{(1 - e^{-b})^2} + \frac{B}{m^{3/2}} \sum_{n=1}^{\infty} n e^{-\beta m(n/m-1)^2} + \frac{C e^{-d/m}}{m^2 (1 - e^{-d/m})^2}. \quad (13)$$

Here we have introduced for convenience the dimensionless bulk concentration  $C_b$ , scaled with the equilibrium monomer concentration  $\mathfrak{X}_1^*$ .

It was shown in Griffiths *et al.*<sup>6</sup> that approximating the equilibrium distribution by the simpler representation

$$\frac{\mathfrak{X}_n^*}{\mathfrak{X}_1^*} = \begin{cases} 1 & n = 1, \\ \frac{B}{m^{3/2}} \exp\left(-\beta m(n/m-1)^2\right) + \frac{C}{m^2} \exp(-dn/m) & n \geq 2, \end{cases} \quad (14)$$

as illustrated in Fig. 1, provides no discernible difference to that observed for the distribution (11) (except for the behaviour in the very narrow region of small aggregates). We use this alternative representation in the derivation of our continuum description in §3. In calculating the kinetics of re-equilibration we will initially use the parameters appropriate to the non-ionic surfactant C<sub>10</sub>E<sub>8</sub>, which has a CMC (1 mM) lying in the middle of the range of surfactants typically used in practical applications. We will then explore the effect of varying the parameters describing the surfactant distribution.

### 3 A continuum model

#### 3.1 Introduction

It is usual to solve the infinite system of ordinary differential equations (2), (4) by truncating at a suitably large value of  $n$ . Determining the solution to the resulting system is thus numerically intensive and so it is extremely advantageous to exploit the largeness of the optimal aggregation number,  $m$ , to derive a continuum model for the system, as adopted in Griffiths *et al.* and Richardson *et al.*<sup>6,7,20</sup>

The distribution (14) is appropriately represented by a continuum function for the aggregate concentrations (becoming exact in the limit  $1/m \equiv \varepsilon \rightarrow 0$ ). We thus let  $x = n/m$  and define the continuum order-one function  $Y(n/m) = m^2 \mathfrak{X}_n^* / \mathfrak{X}_1^*$  for  $n \geq 1$ , and treat the monomer concentration separately. The prefactor  $m^2$  is chosen to ensure that  $Y$  is an order-one function when the proportion of surfactant in aggregate form is comparable with

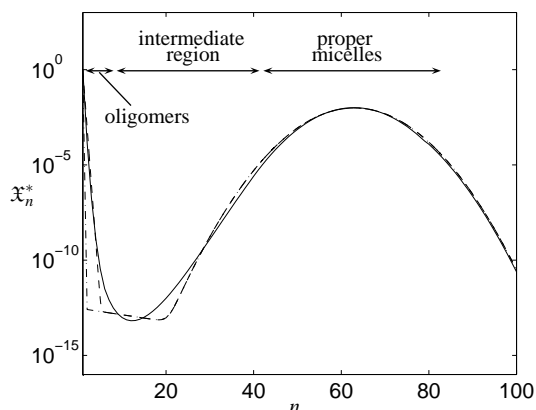


**Fig. 1** An equilibrium aggregate size distribution predicted by MD simulation for the polyoxyethylene glycol alkyl ether surfactant C<sub>10</sub>E<sub>8</sub> at a bulk concentration  $C_b = 10$  mM (solid line).<sup>9</sup> The dashed line shows the fit (11) and the dot-dash line shows the approximation (14), with  $A = 1$ ,  $b = 7$ ,  $B \approx 4.82$ ,  $\beta \approx 0.9$ ,  $m = 63$ ,  $C \approx 3 \times 10^{-13}$ ,  $d \approx 5$ .

the concentration in monomer form. Eqn (14) thus gives

$$Y(x) = \frac{B}{\sqrt{\varepsilon}} \exp\left(-\frac{\beta}{\varepsilon} (x-1)^2\right) + C e^{-dx}. \quad (15)$$

Conservation of mass indicates that

$$1 + \int_0^{\infty} x Y(x) dx = C_b, \quad (16)$$

where  $C_b$  is the dimensionless bulk concentration scaled with  $\mathfrak{X}_1^*$ . By fixing  $\beta$ ,  $\varepsilon$ ,  $C$ ,  $d$  and  $C_b$ , (16) provides the value of  $B$ ,

$$B = \frac{2(C_b d - C) \sqrt{\beta}}{d \sqrt{\pi} \left(1 + \operatorname{erf}\left(\frac{\beta}{\varepsilon}\right)\right)}. \quad (17)$$

We dilute the system by a factor of  $D$  and analyse the evolution of the resulting distribution to the new equilibrium. For simplicity we choose to scale all concentrations with the post-dilution equilibrium monomer concentration, say  $\bar{\mathfrak{X}}_1^* \equiv \nu \mathfrak{X}_1^*$ , where  $\nu = \bar{\mathfrak{X}}_1^* / \mathfrak{X}_1^*$  is the ratio of the pre-dilution to post-dilution monomer concentrations. Provided the system remains micellar,  $\nu$  is typically close to (but slightly less than) unity. This reflects the fact that the monomer concentration is approximately constant (and equal to the CMC) for any bulk concentration that exceeds the CMC, when the system is in micellar form. The scaled initial monomer concentration instantaneously after dilution,  $X_1(0)$ , and new equilibrium dilution,  $\bar{X}_1$ , are then

$$X_1(0) = \frac{1}{\nu D}, \quad \bar{X}_1 = 1. \quad (18)$$

The corresponding initial distribution instantaneously after dilution,  $y_0(x)$ , and new equilibrium distribution,  $\bar{y}(x)$ , are given by Griffiths *et al.*<sup>6,7</sup> as

$$y_0(x) = \frac{Y(x)}{\nu D} = \frac{B_0}{\sqrt{\varepsilon}} \exp\left(-\frac{\beta}{\varepsilon}(x-1)^2\right) + C_0 \exp(-dx), \quad (19a)$$

$$\bar{y}(x) = Y(x) \nu^{x/\varepsilon-1} = \frac{\bar{B}}{\sqrt{\varepsilon}} \exp\left(-\frac{\beta}{\varepsilon}(x-\bar{\omega})^2\right) + \bar{C} \exp(-\bar{d}x), \quad (19b)$$

where the parameters in (19) are related to the pre-dilution distribution by

$$B_0 = \frac{B}{\nu D}, \quad C_0 = \frac{C}{\nu D}, \quad \bar{B} = B \nu^{1/\varepsilon-1} \exp\left(\frac{\log^2 \nu}{4\varepsilon\beta}\right), \\ \bar{C} = \frac{C}{\nu}, \quad \bar{\omega} = 1 + \frac{\log \nu}{2\beta}, \quad \bar{\beta} = \bar{\omega}\beta, \quad \bar{d} = d - m \log \nu. \quad (20)$$

The precise value of  $\nu$  for a dilution by a factor of  $D$  may be determined via the expression for conservation of mass:

$$1 + \int_0^\infty x \bar{y}(x) dx = \frac{C_b}{\nu D}, \quad (21)$$

which may be evaluated explicitly using (19b) to give

$$\frac{C_b}{D} - \nu = \frac{B}{2} \sqrt{\frac{\pi}{\beta}} \bar{\omega} e^{-\beta(1-\bar{\omega})^2/\varepsilon} \left( \frac{1}{\bar{\omega}} \sqrt{\frac{\varepsilon}{\pi\beta}} e^{-\bar{\omega}^2\beta/\varepsilon} + \operatorname{erfc}\left(-\bar{\omega}\sqrt{\frac{\beta}{\varepsilon}}\right) \right) + \frac{C}{\bar{d}^2}, \quad (22)$$

with  $\bar{\omega}$  and  $\bar{d}$  defined in (20).

### 3.2 Governing equations and boundary conditions

Since the concentration of monomer is much larger than the concentration of all other species we choose to separate (2) into reactions involving monomer loss and gain, and reactions involving two general aggregates:

$$\begin{aligned} \frac{d\mathfrak{X}_n}{dt} = & \kappa_{1,1}^+ \mathfrak{X}_1 \mathfrak{X}_{n-1} - \kappa_{1,1}^+ \frac{\mathfrak{X}_1^* \mathfrak{X}_{n-1}^*}{\mathfrak{X}_n^*} \mathfrak{X}_n \\ & - \kappa_{1,1}^+ \mathfrak{X}_1 \mathfrak{X}_n + \kappa_{1,1}^+ \frac{\mathfrak{X}_1^* \mathfrak{X}_n^*}{\mathfrak{X}_{n+1}^*} \mathfrak{X}_{n+1} \\ & + \sum_{i=2}^{n-1} \frac{1}{2} k_{i,n-i}^+ \left( \mathfrak{X}_i \mathfrak{X}_{n-i} - \frac{\mathfrak{X}_i^* \mathfrak{X}_{n-i}^*}{\mathfrak{X}_n^*} \mathfrak{X}_n \right) \\ & - \sum_{i=2}^\infty k_{i,n}^+ \left( \mathfrak{X}_i \mathfrak{X}_n - \frac{\mathfrak{X}_i^* \mathfrak{X}_n^*}{\mathfrak{X}_{i+n}^*} \mathfrak{X}_{i+n} \right), \end{aligned} \quad (23)$$

where we have used (10) to eliminate  $\kappa_{i,j}^-$  and we recall we have chosen  $\kappa_{1,n}^+ = \kappa_{1,1}^+$ . We then set  $y(n/m, t) = m^2 \mathfrak{X}_n(t) / \nu \mathfrak{X}_1^*$  and  $t = t / \varepsilon \kappa_{1,1}^+ \nu \mathfrak{X}_1^*$ , and Taylor expand terms in (23) for small  $\varepsilon$  to yield the continuum representation of (23)

$$\begin{aligned} \frac{\partial y}{\partial t} = & (1 - X_1) \frac{\partial y}{\partial x} + \frac{\varepsilon}{2} (1 + X_1) \frac{\partial^2 y}{\partial x^2} - \varepsilon \frac{\partial}{\partial x} \left( \frac{y'}{\bar{y}} y \right) \\ & + \int_0^x \frac{1}{2} k(s, x-s) \left( y(s, t) y(x-s, t) - \frac{\bar{y}(s) \bar{y}(x-s)}{\bar{y}(x)} y(x, t) \right) ds \\ & - \int_0^\infty k(s, x) \left( y(s, t) y(x, t) - \frac{\bar{y}(s) \bar{y}(x)}{\bar{y}(s+x)} y(s+x, t) \right) ds. \end{aligned} \quad (24a)$$

Here

$$k(i/m, j/m) = \frac{\kappa_{i,j}^+}{\kappa_{1,1}^+},$$

which represents the possibility of the fusion of two aggregates. In the case when we permit only monomer loss or gain,  $k(\xi, \eta) = 0$  for all  $\xi, \eta$  and we recover the governing continuum description for the Becker–Döring equations derived in Griffiths *et al.*<sup>6,7</sup>

The continuum version of (4) is

$$X_1(t) = 1 - \int_0^\infty x (y(x, t) - \bar{y}(x)) dx. \quad (24b)$$

The appropriate boundary conditions for the system (24) are given by,<sup>6</sup>

$$y(0, t) = X_1^2 \bar{y}(0), \quad y \rightarrow 0 \text{ as } x \rightarrow \infty, \quad (25a, b)$$

which capture the behaviour near the monomer spike and ensure that the total amount of surfactant is finite, and the initial post-dilution condition is

$$X_0 = \frac{1}{\nu D}, \quad y_0(x) = \frac{B_0}{\sqrt{\varepsilon}} \exp\left(-\frac{\beta}{\varepsilon}(x-1)^2\right) + C_0 \exp(-dx). \quad (26)$$

We consider the evolution of a surfactant solution with an initial distribution given by (15) following a dilution that leaves the system micellar. We choose to solve the system (24) subject to the boundary conditions (25) and initial post-dilution condition (26) via the method of lines, discretizing space and using the variable coefficient ODE solver VODE.<sup>21</sup>

As demonstrated in Griffiths *et al.*<sup>6,7</sup>, allowing only for monomer loss or gain with  $k(\xi, \eta) = 0$  for all  $\xi, \eta$  leads to re-equilibration times far longer than observed experimentally. In the remainder of the paper we discuss realistic mechanistic routes for re-equilibration following dilution to determine a sensible form for the association rate constants, and thus expression for  $k(\xi, \eta)$ , that yields re-equilibration timescales that are in agreement with experiment.

## 4 Alternative pathways to re-equilibration

### 4.1 Sub-micellar fission

The formation of ionic micellar aggregates was proposed by Kahlweit<sup>22</sup> to take place not only via stepwise monomer gain but through the combination of aggregates. Initially, ionic repulsion causes the overall formation process to occur through stepwise monomer gain, but as the aggregates grow, the effect of the electrical double layer is reduced, allowing larger aggregates to fuse together. Since all reactions must be reversible, this suggests that an alternative route for the breakdown and subsequent re-equilibration of micelles may be offered by the fission of sub-micellar aggregates. This provides two distinct reaction pathways for the breakdown of micelles: one via stepwise monomer loss from aggregates (as described by Becker–Döring theory) and a second via their fission into smaller aggregates.

Fusion of aggregates may be represented mathematically by setting  $\kappa_{i,j}^+$  to be non-zero for  $i, j \neq 1$ . However, to prevent the coalescence of two aggregates to form a species larger than a proper micelle,  $\kappa_{i,j}^+$  must only be non-zero when  $i + j < m$ . In the continuum description, this corresponds to setting  $k(\xi, \eta) = 0$  for  $\xi + \eta > 1$  and  $k(\xi, \eta) = \delta \neq 0$  otherwise, where  $\delta \leq 1$  represents the magnitude of the activation barrier presented for the fusion of two aggregates relative to the fusion of an aggregate and a monomer. For simplicity we suppose here that  $\delta$  is constant and examine the system behaviour governed by (24) following a dilution. We find that, even when  $\delta = 1$  and no activation barrier is present, for realistic aggregate distributions, accounting for this additional mechanistic route yields no discernible difference to the behaviour when  $k(\xi, \eta) \equiv 0$  for all  $\xi, \eta$  and only monomer loss or gain is permitted (Fig. 2). One reason that micelle fission is not a significant pathway is that the maximum in the free energy curves as a function of aggregation number is much less than half the mean aggregation number. Consequently, one or both of the aggregates formed by fission of proper micelles will tend to relax by accretion of monomers to reform a proper micelle. As detailed in Griffiths *et al.*<sup>6,7</sup>, the system initially responds to the dilution by a rapid loss of monomers from the proper micelles which shifts the peak of the micelle size distribution to lower aggregation numbers while the monomer concentration rises, in the  $\tau_1$  process. The system then relaxes to a highly stable *pseudo-equilibrium* state, returning to equilibrium over an exponentially longer timescale, as a result of the high energy barrier set by the extremely low concentration of smaller aggregates. In fact we find that we must set  $C \gtrsim 10^{-4}$  before realistic re-equilibration times are observed (Fig. 3). This corresponds to aggregate distributions for which the ratio of concentration of intermediate aggregates to proper micelles is typically  $10^{-7}$ , many orders of magnitude larger

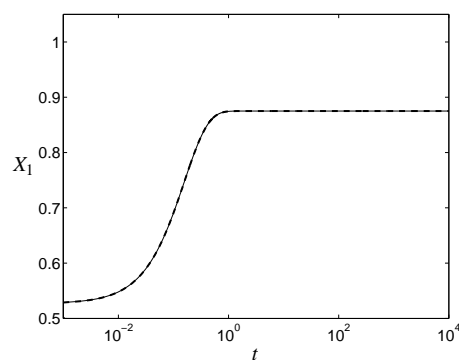


**Fig. 2** Evolution of monomer concentration,  $X_1$ , with time for an initial pre-dilution distribution given by (15) with  $C_b = 10$ ,  $B$  given by (17),  $\beta = 0.9$ ,  $m = 63$ ,  $C = 3 \times 10^{-13}$ ,  $d = 5$  and  $D = 2$ , with:  $k(\xi, \eta) = 0$  for all  $\xi, \eta$  (dashed); and  $k(\xi, \eta) = 1$  for  $\xi + \eta < 1$  and  $k(\xi, \eta) = 0$  otherwise (solid).

than we would expect for  $C_{10}E_8$ , but which might be reached for surfactants with much higher CMCs.

Hence incorporating the fusion and fission of only small aggregates does not enable micelle breakdown to occur on a sensible timescale. It is thus evident that micelle breakdown is unable to occur via any method that involves aggregates passing through the high energy region of intermediate aggregate sizes, and so there must be an alternative route to equilibrium.

### 4.2 Super-micelle formation

In this section we explore the possibility of permitting the combination of two aggregates to form an aggregate larger than a proper micelle as a possible route to equilibrium. Although it is rare that any attention is paid to the region beyond the proper micelles, the aggregation of two micelles to form transient larger species has been demonstrated experimentally for the surfactant Triton X-100.<sup>23,24</sup> In this case such aggregates persist at least for the time interval necessary for exchange of the solubilized pyrene-labelled triglyceride tracer molecule. While it is shown that the formation of these larger aggregates, which we shall term *super-micelles*, occurs at a rate approximately 5000 times less than the diffusion-controlled rate, such a rate is still remarkably fast when considering the necessary re-organization required for aggregate merging. The kinetics of micellar formation has very recently been studied via a free-energy approach by Hadgiivanova *et al.*<sup>25</sup>. Here it was shown that micelles form via a series of stages on well-separated timescales, beginning with the conventional nucleation of monomers to form critical aggregates, but then switching mechanism to a lower energy route to reach the resultant equilibrium. In some cases this second process

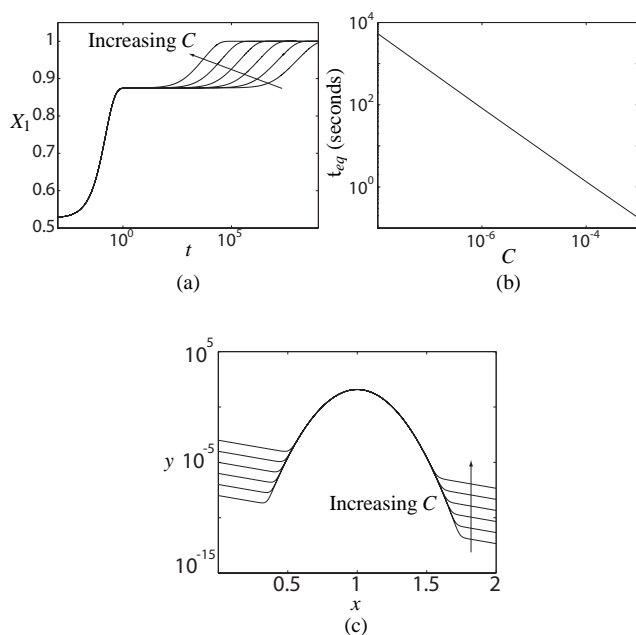


**Fig. 3** (a) Evolution of monomer concentration,  $X_1$ , with time for an initial pre-dilution distribution given by (15) with  $C_b = 10$ ,  $B$  given by (17),  $m = 63$ ,  $\beta = 0.9$ ,  $d = 5$ ,  $D = 2$ ,  $k(\xi, \eta) = 1$  for  $\xi + \eta < 1$  and  $k(\xi, \eta) = 0$  otherwise, and  $C = 10^{-3}, 10^{-4}, 10^{-5}, 10^{-6}, 10^{-7}$ , and  $10^{-8}$ ; (b) Dependence on  $C$  of real time taken for the distribution in (a) to reach equilibrium, chosen to be the time at which  $X_1$  reaches 0.99,  $t_{eq} \approx 7 \times 10^{-3} C^{-0.822}$  seconds. The corresponding pre-dilution distributions are shown in (c).

was shown to involve the formation of aggregates that exceed the size of a proper micelle, which subsequently break down to complete the formation of the proper micelles.

We account for the coagulation of aggregates to form species that exceed the size of a proper micelle by setting  $k(\xi, \eta) = \text{constant} = \delta$  for all  $\xi, \eta$ , where  $\delta \leq 1$  again corresponds to the magnitude of the activation barrier. The system dynamics illustrated in Fig. 4 clearly show a marked increase in the concentration of aggregates generated that exceed the size of a proper micelle when compared with the evolution via stepwise monomer loss or gain alone. Hence a proportion of super-micelles are indeed formed via the fusion of aggregates that lie to the left of the equilibrium aggregation number when such reactions are permitted. Once formed, these super-micelles break down quickly via a cascade of monomer release due to their instability. However, crucially, as displayed in Fig. 5, the timescale of re-equilibration via this new mechanism is now much faster than via monomer loss alone, even for the case when  $\delta = 1/5000$  and the merging of aggregates occurs at a rate 5000 times more slowly than the diffusion-controlled rate of monomer gain as predicted by Rharbi *et al.*<sup>23,24</sup>. As a result, unlike the stepwise monomer loss model

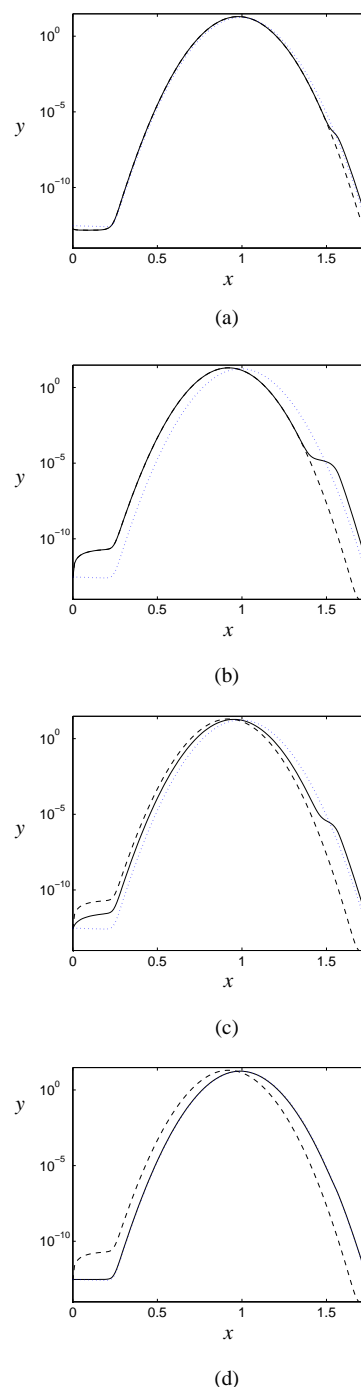


**Fig. 4** Evolution of an initial pre-dilution distribution given by (15) with  $C_b = 10$ ,  $B$  given by (17),  $\beta = 0.9$ ,  $m = 63$ ,  $C = 3 \times 10^{-13}$ ,  $d = 5$ , and  $D = 2$ , with  $k(\xi, \eta) = 1/5000$  at (a)  $t = 0.05$ , (b) 10, (c)  $1.5 \times 10^4$ , (d)  $5 \times 10^4$  (each depicted by the solid line) towards the equilibrium distribution (dotted curve). The dashed curve shows the profile at equivalent times when  $k(\xi, \eta) = 0$ , corresponding to re-equilibration through monomer loss or gain only, which fails to reach the equilibrium distribution.

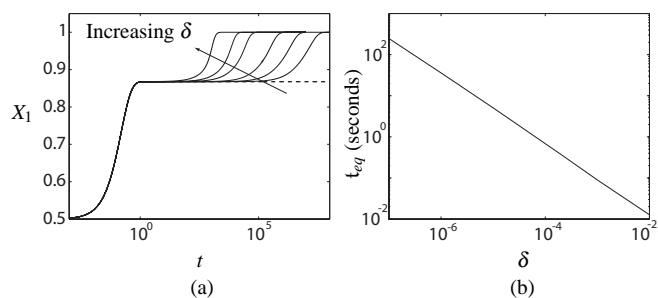


**Fig. 5** (a) Evolution of monomer concentration,  $X_1$ , with time for an initial pre-dilution distribution given by (15) with  $C_b = 10$ ,  $B$  given by (17),  $\beta = 0.9$ ,  $m = 63$ ,  $C = 3 \times 10^{-13}$ ,  $d = 5$  and  $D = 2$ , with  $k(\xi, \eta) = \delta = 10^{-7}, 10^{-6}, 10^{-5}, 2 \times 10^{-4}, 10^{-3}, 10^{-2}$ . The case when  $\delta = 0$  which corresponds to monomer loss or gain alone is shown by the dashed curve; (b) Dependence on  $\delta$  of real time taken for the distribution in (a) to reach equilibrium, chosen to be the time at which  $X_1$  reaches 0.99,  $t_{eq} \approx 2.44 \times 10^{-4} \delta^{-0.858}$  seconds.

governed by Becker–Döring theory, this additional pathway for re-equilibration now allows the system to re-equilibrate on a timescale of the order of seconds, in line with stopped-flow experiments.<sup>9</sup> Fusion of proper micelles to form supermicelles is not restricted to non-ionic surfactants, but has also been observed in MD simulations of the ionic surfactant decyltrimethylammonium bromide.<sup>16</sup>

The distinct two-timescale evolution of the system during re-equilibration is still clearly present in Fig. 5. A rapid rise in monomer concentration over an order-one timescale (corresponding to the  $\tau_1$  process), before reaching a plateau below the equilibrium value at which the concentration remains relatively constant, is followed by a recommencement in the journey towards the equilibrium concentration at a slower pace (the  $\tau_2$  process). We notice that the system evolution during the  $\tau_1$  process and the monomer concentration attained at the plateau are almost entirely unaffected by allowing for supermicelle formation. Hence we conclude that this process becomes significant only on the  $\tau_2$  timescale of re-equilibration. As the relative activation barrier,  $\delta$ , is reduced, the time taken to reach equilibrium is reduced, as we would anticipate, and is shown to follow a simple power-law relation in Fig. 5(b). The exponent found is slightly smaller than  $-1$  since not all supermicelles decay by sequential monomer loss. As  $\delta$  increases, so does the probability of fission of a super-micelle back into two proper micelles.

### 4.3 Limitations of the Becker–Döring theory

While it is clear that Becker–Döring theory explains the  $\tau_1$  process it is important to determine the regimes for which this reduced model provides an accurate description of the

entire system behaviour. As discussed, re-equilibration via stepwise monomer loss is significantly compromised when the concentration of aggregates in the intermediate region is low. The evolution predicted by Becker–Döring theory is shown to provide an accurate description of the behaviour observed when we allow all possible reactions (by setting  $k(\xi, \eta) = \delta = 1/5000$ ) when  $C$  is suitably large ( $\gtrsim 10^{-3}$ ) and the relative concentration of intermediate aggregates to proper micelles is not too low (around  $10^{-6}$ ) (Fig. 6(a,b)). In this case the re-equilibration process favours the route of entire micelle breakdown through stepwise monomer loss. However, as  $C$  increases and the relative concentration of intermediate aggregates is reduced further, the deviation between the predicted evolution by the Becker–Döring theory and that when all aggregation reactions are permitted increases and Becker–Döring theory becomes less valid (Fig. 6(c,d)). This demonstrates that the route to equilibrium offered by stepwise monomer loss rapidly becomes unfeasible when the relative concentration of intermediate aggregates is small. The structural composition of the majority of surfactant species is such that the probability of existing as an intermediate aggregate is typically many orders of magnitude lower than the distributions considered in Fig. 6. As a result Becker–Döring theory is likely to fail to describe the re-equilibration of a wide spectrum of realistic surfactant systems. Thus our new theory is essential, providing a description of the re-equilibration behaviour of *any* surfactant distribution, with the Becker–Döring theory forming a subset of our model.

We have shown that, although the energetic favourability of the coagulation of two sub-micellar aggregates to form a super-micelle is low, this process is still able to generate a non-negligible proportion of super-micelles that subsequently allow re-equilibration via rapid monomer loss. However, the nature of the surfactant distribution and the relative favourabilities of the different aggregates suggests that only a small proportion of aggregates smaller than proper micelles are likely to play a part in the re-equilibration mechanism: the energy penalty for the coagulation of two larger aggregates grows rapidly with increasing aggregate size, while the concentration of smaller aggregates quickly falls with decreasing size. This supposition may be confirmed by reducing the number of additional aggregate reactions that are allowed. In Fig. 7 we compare the re-equilibration behaviour exhibited when  $k(\xi, \eta) = 1/5000$  when  $0.63 < \xi, \eta < 0.74$  and  $k(\xi, \eta) = 0$  otherwise with the behaviour when  $k(\xi, \eta) = 1/5000$  for all values of  $\xi, \eta$  and we see that the behaviour is essentially identical. This confirms that only aggregates that lie in a small range, centred about a typical aggregation number of around 70% of the size of a proper micelle, actually contribute to the super-micelle route to equilibrium.

The width of the region of stable proper micelles may be reduced by increasing either the value of  $\beta$  or  $m$  while retain-

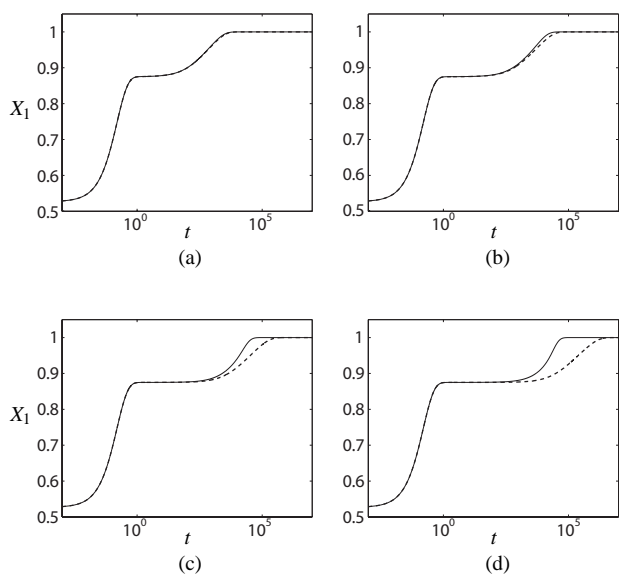


**Fig. 6** Evolution of monomer concentration,  $X_1$ , with time for an initial pre-dilution distribution given by (15) with  $C_b$   $B$  given by (17),  $\beta = 0.9$ ,  $m = 63$ ,  $d = 0.2$  and  $D = 2$  and (a)  $C = 10^{-2}$ , (b)  $C = 10^{-3}$ , (c)  $C = 10^{-4}$ , (d)  $C = 10^{-5}$ . In each figure the solid line shows the evolution when  $k(\xi, \eta) = \delta = 1/5000$  and the dashed line the evolution when  $k(\xi, \eta) = 0$ .

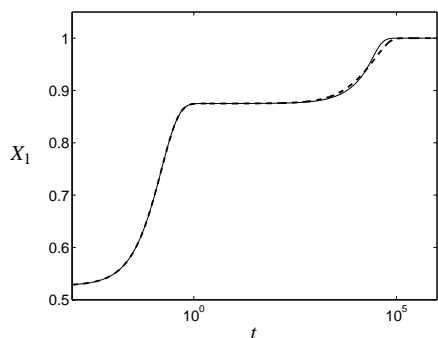


**Fig. 7** Evolution of monomer concentration,  $X_1$ , with time for an initial pre-dilution distribution given by (15) with  $C_b = 10$ ,  $B$  given by (17),  $\beta = 0.9$ ,  $m = 63$ ,  $C = 3 \times 10^{-13}$ ,  $d = 5$ , and  $D = 2$ , with  $k(\xi, \eta) = \delta = 1/5000$  for all  $\xi, \eta$  (solid), and  $k(\xi, \eta) = 1/5000$  for  $0.63 < \xi, \eta < 0.74$  and  $k(\xi, \eta) = 0$  otherwise (dashed).

ing the bulk concentration and relative proportions of micellar and intermediate aggregates. In both cases we uncover a simple power-law relation for the dependence of the time to equilibration on the two respective parameters as illustrated in Figs. 8(d) and 9(c). Upon varying  $\beta$  we find that the value of the monomer concentration attained at pseudo-equilibrium following the  $\tau_1$  process is also shown to be reduced. On the other hand, as the value of  $\beta$  is reduced we find the relative concentration of aggregates in the intermediate region rises (as depicted in Fig. 8(c)), and a switch in the favourable re-equilibration route from super-micelle formation to conventional stepwise monomer loss will take place. Surfactants with short alkyl chains (especially so for ionic surfactants) tend to have high CMCs, small aggregation numbers and broad distributions (which corresponds to small values of  $\beta$ ) all of which favour relaxation by stepwise monomer loss. The Becker–Döring pathway is therefore more likely to be the dominant relaxation mechanism for such surfactants.

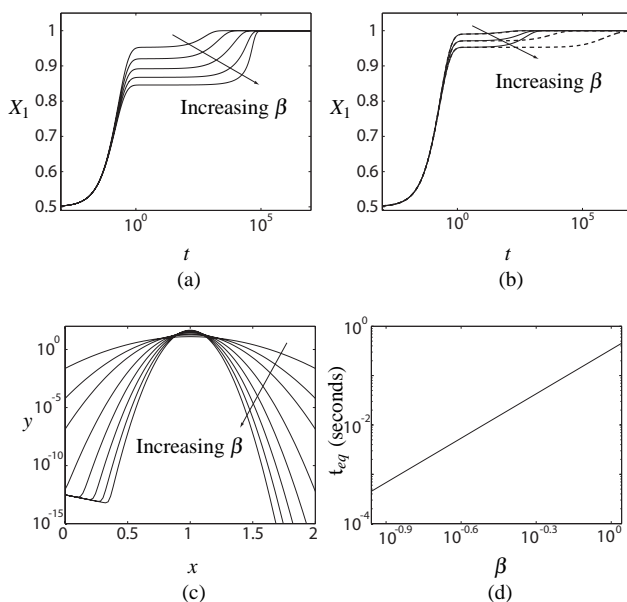


**Fig. 8** Evolution of monomer concentration,  $X_1$ , with time for an initial pre-dilution distribution given by (15) with  $C_b = 10$ ,  $B$  given by (17),  $m = 63$ ,  $C = 3 \times 10^{-13}$ ,  $d = 5$ ,  $D = 2$ ,  $k(\xi, \eta) = \delta = 1/5000$  and (a)  $\beta = 0.5, 0.7, 0.9, 1.1, 1.3$ , (b)  $\beta = 0.1, 0.2, 0.3$ . The dashed curves in (b) show the corresponding evolution when  $\beta = 0.1, 0.2, 0.3$  and  $k(\xi, \eta) = 0$ . The corresponding pre-dilution distributions are shown in (c); (d) Dependence on  $\beta$  of time taken for the distributions in (a) and (b) to reach equilibrium,  $t_{eq} \approx 0.34\beta^3$  seconds.

As we might expect, increasing the dilution factor,  $D$ , results in longer recovery times, since the proportion of proper micelles that must undergo the complex breakdown and super-micelle restructuring processes to replenish the monomer to

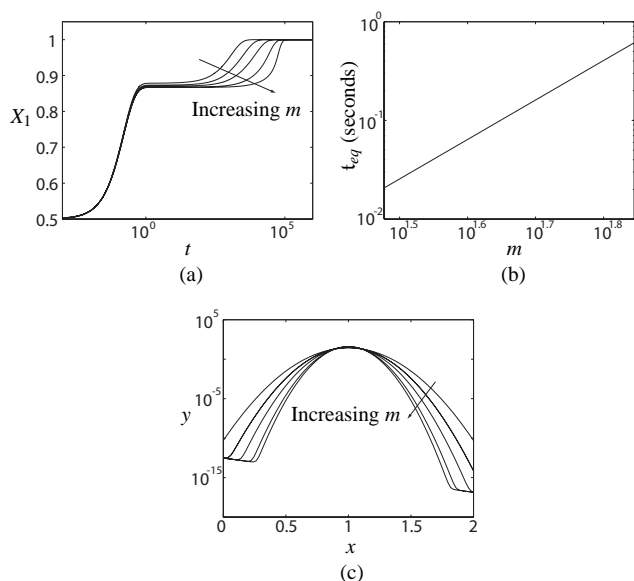


**Fig. 9** (a) Evolution of monomer concentration,  $X_1$ , with time for an initial pre-dilution distribution given by (15) with  $C_b = 10$ ,  $B$  given by (17),  $\beta = 0.9$ ,  $C = 3 \times 10^{-13}$ ,  $d = 5$ ,  $D = 2$  and  $k(\xi, \eta) = \delta = 2 \times 10^{-4}$  and  $m = 30, 40, 50, 63, 70$ ; (b) Dependence on  $m$  of time taken for the distribution in (a) to reach equilibrium, chosen to be the time at which  $X_1$  reaches 0.99,  $t_{eq} \approx 2.55 \times 10^{-8} m^4$  seconds.

the CMC increases (Fig. 10). The time taken for the system to re-equilibrate is shown to follow the power-law relation  $t_{eq} \approx 0.0850D^2$  (seconds). As the bulk surfactant concentration following dilution falls below the CMC and the resulting system is no longer micellar the time taken for the system to attain its equilibrium rises dramatically, deviating from this power-law relation. Adjusting the bulk surfactant concentration leads to a similar result, with the re-equilibration time obeying the power law approximation  $t_{eq} \approx 13.47C_b^{-1.75}$  (seconds) provided the system remains micellar following dilution, and taking significantly longer to re-equilibrate if the solution falls below the CMC following dilution (Fig. 11).

## 5 Conclusions

We studied the mechanism for the re-equilibration following dilution of a surfactant system whose typical concentration of intermediate aggregates in equilibrium is much lower than the typical concentration of proper micelles, as is the case for the majority of real-life surfactants. This process is conventionally assumed to occur via stepwise monomer loss or gain, leading to the well-known Becker–Döring theory. It was shown in Griffiths *et al.*<sup>6,7</sup> that if the restructuring of such a system occurs via this mechanism then the timescales for re-

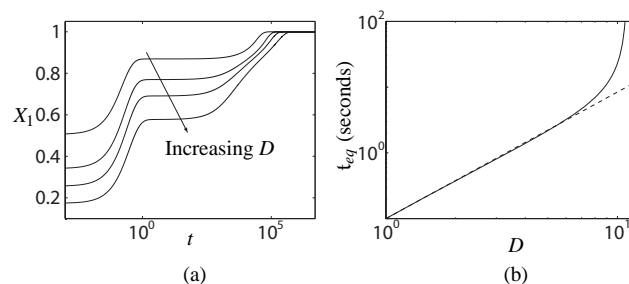


**Fig. 10** Evolution of monomer concentration,  $X_1$ , with time for an initial pre-dilution distribution given by (15) with  $C_b = 10$ ,  $B$  given by (17),  $\beta = 0.9$ ,  $C = 3 \times 10^{-13}$ ,  $d = 5$ ,  $m = 63$ ,  $k(\xi, \eta) = \delta = 2 \times 10^{-4}$  and  $D = 2, 3, 4, 6$ ; (b) Dependence on  $D$  of time taken for the distribution in (a) to reach equilibrium, chosen to be the time at which  $X_1$  reaches 0.99,  $t_{eq}$ . The dotted line shows the fit  $t_{eq} = 0.0850D^2$  seconds.

equilibration are far longer than those observed experimentally for  $C_nE_m$  surfactants.

We exploited the largeness of the typical optimum aggregation number was exploited to enable a continuum approach. This vastly simplified the complexity of the problem, reducing the task from solving a large system of nonlinear coupled ordinary differential equations to a single integro-differential equation governing the aggregate distribution, and an integral relation that provides the monomer concentration.

We relaxed the assumption of stepwise monomer loss or gain and analysed two potential alternative mechanistic routes to equilibrium. Firstly, we allowed for micelles to break down into smaller aggregates, the reverse route of which was shown by Kahlweit<sup>22</sup> to be key in the formation of ionic micelles. However, this situation was shown to produce no discernible difference when compared with solutions to the original Becker–Döring theory. Re-equilibration was thus concluded to be unable to proceed via any mechanistic route that involves the low-concentration region of intermediate aggregates.

Secondly, we allowed for the combination of aggregates to form *super-micelles*, that is, aggregates that are larger than proper micelles and are thus much more unstable. Although the role of super-micelles is generally ignored when studying re-equilibration behaviour, recent experimental observations of the formation of such species suggest that such reactions are at least possible.<sup>23,24</sup> The early time behaviour of the system during the  $\tau_1$  process was shown to be almost entirely unaffected by the allowance of super-micelle formation. Here the behaviour is dominated by the stepwise monomer release from micelles, which is well-represented by the simpler Becker–Döring theory. However, super-micelles, which form by the fusion of aggregates smaller than proper micelles, were

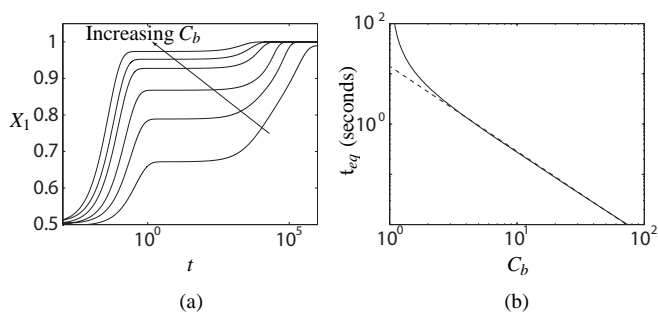


**Fig. 11** (a) Evolution of monomer concentration,  $X_1$ , with time for an initial pre-dilution distribution given by (15) with  $\beta = 0.9$ ,  $C = 3 \times 10^{-13}$ ,  $d = 5$ ,  $m = 63$ ,  $k(\xi, \eta) = \delta = 2 \times 10^{-4}$  and  $C_b = 2, 5, 10, 20, 30, 50$  and  $B$  given by (17); (b) Dependence on  $C_b$  of time taken for the distribution in (a) to reach equilibrium, chosen to be the time at which  $X_1$  reaches 0.99,  $t_{eq}$ . The dotted line shows the fit  $t_{eq} \approx 19C_b^{-1.8}$  seconds.

found to play a vital role during the  $\tau_1$  process when some of the aggregates must supply monomers to the remaining aggregates to increase their aggregation number and stability. The instability of these super-micelles led to their rapid breakdown via stepwise monomer loss to produce stable proper micelles while simultaneously driving the monomer concentration back to the CMC.

Conventional entire micelle breakdown via stepwise monomer loss, and re-equilibration via the formation of super-micelles which rapidly dissociate by stepwise monomer loss into proper micelles and monomers, thus provide two possible routes to achieving equilibrium. Allowing for both pathways leads to system re-equilibration on timescales that are consistent with those observed in practice, for example via stopped-flow experiments. The second route is accelerated by monomer depletion and the corresponding shift to smaller aggregation numbers that follows a dilution, but, unlike the Becker–Döring mechanism, is still possible even when the concentration of aggregates in the intermediate region is extremely small. The time taken for the system to re-equilibrate via this new mechanism was shown to depend on the key parameters via simple power-law relations.

The combination of much lower concentrations of smaller aggregates and the energetic unfavourability of the fusion of larger aggregates for typical surfactant systems results in only a narrow range of aggregate sizes that are actually able to participate in super-micelle formation. We showed these aggregates to be localized to a small window centred around aggregates typically 70% of the size of a proper micelle.

We examined the regimes under which the conventional Becker–Döring description sensibly describes the breakdown and re-equilibration of aggregates in a micellar solution. For

systems where the relative concentration of intermediate aggregates is no less than around six orders of magnitude smaller than the concentration of proper micelles, Becker–Döring theory provides an accurate description of the system behaviour predicted by the full model that allows for aggregate fusion. The Becker–Döring system is thus a subset of our new theory, which describes the re-equilibration of *any* surfactant distribution. However, the energetic favourability of surfactant aggregates is such that in practice the proportion of surfactant residing in the form of intermediate aggregates is typically many orders of magnitude lower than that considered here. As a result, those regimes that the Becker–Döring theory are able to accurately describe are unlikely to represent the distribution and thus re-equilibration behaviour of the majority of surfactant systems in practical use. This therefore rules out stepwise monomer loss as a universal route to equilibrium, rendering super-micelle formation a new but essential mechanistic route in the overall re-equilibration of a micellar surfactant solution following dilution.

Implicit in our model is that the formation of micelles in a supersaturated solution proceeds by accretion of monomers to a proper micelle to form a super-micelle followed by fission of the super-micelle to two proper micelles; the formation of micelles is catalyzed by micelles. For typical surfactants, extreme levels of supersaturation would be required to form a micelle by the Becker–Döring mechanism, so it is likely that the first micelles are formed by a heterogeneous mechanism, as is common in most nucleation processes.

## A A comment on the values of $\kappa_{i,j}^-$

The ratio of the rate constants for formation of super-micelles from two micelles, and for fission of a super-micelle, is determined by the equilibrium constant for the reaction. The rate constant for fission cannot rise without bound, however, since it is constrained by the time taken for the surfactants to reorganize on a microscopic scale. A practical upper bound on  $\kappa_{i,j}^-$  is  $10^{10} \text{ s}^{-1}$ , corresponding to a reorganization time of 0.1 ns. We have calculated the implicit fission rate constant for diffusion-controlled micelle fusion ( $\delta = 1$ ) as a function of micelle size for the surfactant  $C_{10}E_8$  with distribution shown in Fig. 1. We find that the fission rate constant is less than  $10^{10} \text{ s}^{-1}$  for all processes leading to super-micelles with aggregation numbers less than 100. For a value of  $\delta = 1/5000$ , all processes involving super-micelles up to a size of around 112 have physically reasonable rate constants. However, we have shown that the reactions that are responsible for the super-micelle route to equilibrium are those involving the fusion of aggregates with sizes 63–74% of the size of a proper micelle (which correspond to aggregation numbers of 40–47 for the surfactant  $C_{10}E_8$ ). Such reactions thus fall within the maximum values

---

for dissociation rates that could be realistically expected, even when we assume diffusion-limited aggregation for all reactions and no activation barrier is present for the fusion of two aggregates.

## References

- 1 M. J. Rosen, *Surfactants and Interfacial Phenomena*, Wiley, (2004).
- 2 E. A. G. Aniansson and S. N. Wall, *J. Phys. Chem.*, 1974, **78**, 1024–1030.
- 3 E. A. G. Aniansson and S. N. Wall, *J. Phys. Chem.*, 1975, **79**, 857–858.
- 4 E. A. G. Aniansson, S. N. Wall, M. Almgren, H. Hoffmann, I. Kielmann, W. Ulbricht, R. Zana, J. Lang and C. Tondre, *J. Phys. Chem.*, 1976, **80**, 905–922.
- 5 R. Nagarajan and E. Ruckenstein, *Langmuir*, 1991, **7**, 2934–2969.
- 6 I. M. Griffiths, C. D. Bain, C. J. W. Breward, D. M. Colegate, P. D. Howell and S. L. Waters, *J. Coll. Int. Sci.*, 2011, **360**, 662–671.
- 7 I. M. Griffiths, C. D. Bain, C. J. W. Breward, S. J. Chapman, P. D. Howell and S. L. Waters, *SIAM J. Appl. Math.*, 2012, **72**, 201–215.
- 8 H. Hoffmann, R. Nagel, G. Platz and W. Ulbricht, *Coll. Polymer Sci.*, 1978, **254**, 812–834.
- 9 D. M. Colegate, *PhD thesis*, Structure-kinetics relationships in micellar solutions of nonionic surfactants, Durham University, 2009.
- 10 V. Smoluchowski, *Phys. Chem*, 1917, **92**, 129–168.
- 11 R. Becker and W. Döring, *Ann. Phys.*, 1935, **24**, 719–752.
- 12 M. Smoluchowski, *Phys. Zeits.*, 1916, **17**, 557–565.
- 13 M. Teubner, *J. Phys. Chem.*, 1979, **83**, 2917–2920.
- 14 T. Yasunaga, K. Takeda and S. Harada, *J. Coll. Int. Sci.*, 1973, **42**, 457–463.
- 15 J. N. B. de Moraes and W. Figueiredo, *Physica Status Solidi*, 2001, **187**, 57–62.
- 16 M. Jorge, *Langmuir*, 2008, **24**, 5714–5725.
- 17 G. Mohan and D. I. Kopelevich, *J. Chem. Phys.*, 2008, **128**, 044905.
- 18 R. Nagarajan and E. Ruckenstein, *J. Coll. Int. Sci.*, 1979, **71**, 580–604.
- 19 S. Puvvada and D. Blankschtein, *J. Chem. Phys.*, 1990, **92**, 3710.
- 20 G. Richardson, L. J. Cummings, H. J. Harris and P. O'Shea, *Biophysical Journal*, 2007, **92**, 4145–4156.
- 21 P. N. Brown, G. D. Byrne and A. C. Hindmarsh, *SIAM J. Sci. Stat. Comput.*, 1989, **10** (5), 1038–1051.
- 22 M. Kahlweit, *J. Coll. Int. Sci.*, 1982, **90**, 92–99.
- 23 Y. Rharbi, M. Li, M. A. Winnik and K. G. Hahn Jr, *J. Am. Chem. Soc.*, 2000, **122**, 6242–6251.
- 24 Y. Rharbi, M. A. Winnik and K. G. Hahn Jr, *Langmuir*, 1999, **15**, 4697–4700.
- 25 R. Hadgiivanova, H. Diamant and A. D., *J. Phys. Chem. B*, 2011, **115**, 7268–7280.



## RECENT REPORTS

12/59	Numerical simulation of shear and the Poynting effects by the finite element method: An application of the generalised empirical inequalities in non-linear elasticity	Mihai Goriely
12/60	From Brownian dynamics to Markov chain: an ion channel example	Chen Erban Chapman
12/61	Three-dimensional coating and rimming flow: a ring of fluid on a rotating horizontal cylinder	Leslie Wilson Duffy
12/62	A two-pressure model for slightly compressible single phase flow in bi-structured porous media	Soulaine Davit Quintard
12/63	Mathematical modelling plant signalling networks	Muraro Byrne King Bennett
12/64	A model for one-dimensional morphoelasticity and its application to fibroblast-populated collagen lattices	Menon Hall McCue McElwain
12/65	Effective order strong stability preserving RungeKutta methods	Hadjimichael Macdonald Ketcheson Verner
12/66	Morphoelastic Rods Part I: A Single Growing Elastic Rod	Moulton Lessinnes Goriely
12/67	Wrinkling in the deflation of elastic bubbles	Aumaitre Knoche Cicuta Vella
12/68	Indentation of ellipsoidal and cylindrical elastic shells	Vella Ajdari Vaziri Boudaoud
12/69	Memory of Recessions	Cross McNamara Pokrovskii
12/70	An estimate of energy dissipation due to soil-moisture hysteresis	McNamara
12/71	The Mathematics Behind Sherlock Holmes: A Game of Shadows	Goriely Moulton
12/72	Some observations on weighted GMRES	Güttel Pestana
12/73	Bounds on the solution of a Cauchy-type problem involving a	Furati

12/75	Error estimation and adaptivity for incompressible, nonlinear (hyper)elasticity	Whiteley Tavener
12/76	A note on heat and mass transfer from a sphere in Stokes flow at low Péclet number	Bell Byrne Whiteley Waters
12/77	Effect of disjoining pressure in a thin film equation with non-uniform forcing	Moulton Lega
12/78	A Review of Mathematical Models for the Formation of Vascular Networks	Scianna Bell Preziosi
12/79	Fast and Accurate Computation of Gauss-Legendre and Gauss-Jacobi Quadrature Nodes and Weights	Hale Townsend
12/80	On the spectral distribution of kernel matrices related to radial basis functions	Wathen Zhu
12/81	Inner product computation for sparse iterative solvers on distributed supercomputer	Zhu Gu Liu

**Copies of these, and any other OCCAM reports can be obtained from:**

**Oxford Centre for Collaborative Applied Mathematics  
Mathematical Institute  
24 - 29 St Giles'  
Oxford  
OX1 3LB  
England  
[www.maths.ox.ac.uk/occam](http://www.maths.ox.ac.uk/occam)**